Electronic Supporting Information

SO_x-modified porous carbon as highly active electrocatalyst for efficient H_2O_2 generation

*Kunhong Jiang ‡[a], Zhenyu Li ‡[ab], Ying Yu [a], Jiefei Li [a], Zhuoyuan Ma [c], Hang Wei *[a], and Haibin Chu*[a]*

[a] College of Chemistry and Chemical Engineering, Inner Mongolia Engineering and Technology Research Center for Catalytic Conversion and Utilization of Carbon Resource Molecules, Inner Mongolia University, Hohhot 010021, PR China

[b] State Key Laboratory of Catalysis, Dalian National Laboratory for Clean Energy, Dalian Institute of Chemical Physics, Chinese Academy of Sciences, Dalian, 116023, China

[c] College of Chemistry, Jilin University, Changchun 130022, PR China

* Corresponding Authors.

E-mail addresses: weihang@imu.edu.cn (H. Wei), chuhb@imu.edu.cn (H. Chu).

[1] K. Jiang and Z. Li contributed equally to this work.

Experimental Section

Materials: 2-Hydroxyethyl methacrylate (HEMA), tetraethyl orthosilicate (TEOS), phenylbis(2,4,6-trimethylbenzoyl)phosphine oxide (819), carbon disulfide, and hydrofluoric acid (40%) were purchased from Aladdin (analytically pure grade). All chemicals and reagents were used directly without the further purification process.

Preparation of SO_x-Porous C: 3.0 g of HEMA and 0.084 g of 819 were added into a beaker, and then stirred until completely dissolved. Subsequently, 150 mg of TEOS and different amounts of CS_2 were added to the above solution. After being stirred, the precursor was transferred into the porcelain combustion boat under a UV-curing reaction. The UV-curing process was straightforward; that, the required precursors were exposed under UV light. Then the liquid precursor was transformed into solid very quickly, and all the components in the precursor were uniformly mixed at a molecular level. The SO_x-porous C was obtained after calcining the above solid precursor in a tubular furnace under a nitrogen atmosphere for 400 °C for 1 h and 700 °C for 1 h with a heating rate of 5 °C min^{-1}, respectively. The achieved black powder was treated with HF (40%) for 24 h. The preparation process of porous carbon sample is the same as porous SO_x-C catalyst, just without the addition of CS_2. The procedure for synthesizing the catalysts and ORR reaction pathways is illustrated in Figure S1.

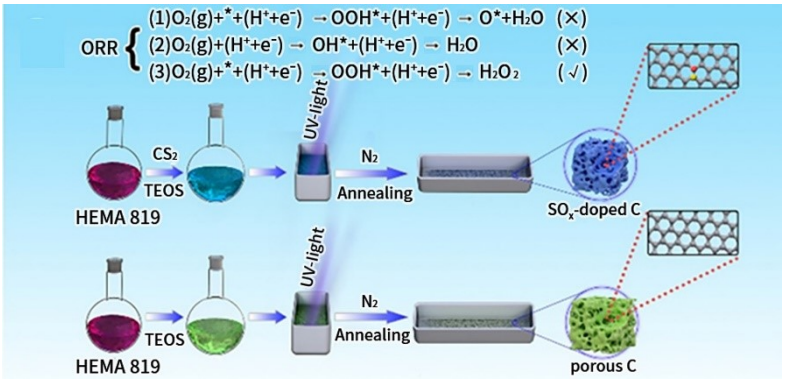

Figure S1 Schematic illustration of the catalysts and ORR reaction pathways.

Characterizations: Powder X-Ray diffraction (XRD) patterns were collected on a Bruker D8 Advance diffractometer using Cu Kα irradiation (λ=1.5406 Å). Raman spectra were measured by the LabRAM HR Evolution Raman spectrometer. N_2 adsorption-desorption curves (BET) were obtained by automatic mesoporous microporous analyzer BK100C. The composition and morphology of the nanocomposite were characterized by transmission electron microscope (TEM, TECNAI-F20). X-ray photoelectron spectra (XPS) was collected on a THS-103X X-ray photoelectron spectrometer. Fourier transform infrared spectroscopy (FTIR) was performed with a Nicolet Nexuc 670 spectrometer. H_2O_2 concentration was tested on Perkin Elmer Lambda 750 UV spectrophotometer. The static contact angle results were obtained by a Drop Shape Analysis System DSA100.

Electrochemical Measurements: The catalytic performance of the as-prepared SO_x-porous C and porous C catalysts were tested at the CHI 760E electrochemical workstation and the rotary disk facility of Pine Company. A three-electrode system was constructed with an Ag/AgCl electrode as the reference electrode, platinum wire as the counter electrode, and a glassy carbon electrode (GC, diameter 5mm, effective area of 0.196 cm^2) coated with catalyst as the working electrode. The 5 mg catalyst was dispersed and treated by ultrasonication in a mixture of 20 μL Nafion (5 wt%), 0.2 mL ethanol, and 0.78 mL deionized water for 40 min to form homogeneous catalyst ink. Subsequently, 27.5 μL of the above ink was transferred to the carbon electrode to prepare the working electrode. The cyclic voltammetry (CV) of the catalyst was tested in 0.1 M N_2-saturated KOH solution at room temperature with the potential range of -

0.8 to 0.3 V (*vs.* Ag/AgCl), and the scanning rate was 50 mV s^{-1}. The H_2O_2 selectivity was obtained by linear sweep voltammetry in 0.1 M KOH solution saturated with O_2 at a rotating speed of 1600 rpm. The stability was determined by CV at a scanning rate of 100 mV s^{-1} in an O_2 saturated solution of 0.1 M KOH at room temperature. The selectivity of hydrogen peroxide measured at the ring disk electrode is determined using the following relation:

$$H_2O_2(\%)=200*I_r/(N*I_d)+I_r$$

The number of transferred electrons measured at the ring disk electrode is based on the equation as follows:

$$n=4*I_d/(I_d+I_r/N)$$

in which I_r is the ring current, I_d is the ring current, and N is the collection efficiency of hydrogen peroxide at the ring electrode (N=0.37).

The synthesis of H_2O_2 was carried out in a three-electrode system with an H-type electrolytic cell separated by a Nafion115 (Dupont) membrane. The platinum wire is used as the counter electrode, and Ag/AgCl as the reference electrode. 5 mg of catalyst is dispersed in 10 μL Nafion (5 wt %), 0.25 mL isopropanol, and 0.74 mL deionized water. The ink was dispersed uniformly by ultrasonication for more than 40 minutes, and then the working electrode can be obtained through evenly coating the carbon paper with a catalyst loading of 0.5 mg cm^{-2}. In a 10 mL O_2-saturated 0.1 M KOH, 1 mL reaction solution was taken at different intervals to identify the concentration of H_2O_2 after the I-t test at 0.5 V vs. RHE.

$TiO(SO_4)$ was used as a chromogenic agent, and UV-visible spectrum was used for the quantitative determination of H_2O_2. The principle of quantitative reaction is based on the chemical equation $Ti^{4+} + H_2O_2 + 2H_2O = H_2TiO_4 + 4H^+$. 0.37g of $TiOSO_4$ was dissolved in 50 mL water. H_2O_2 of known concentration was added to the $TiOSO_4$ solution and measured using UV- visible spectrum, then the calibration curve was obtained. And the concentration of H_2O_2 could be calculated according to the standard curve (Figure S1).

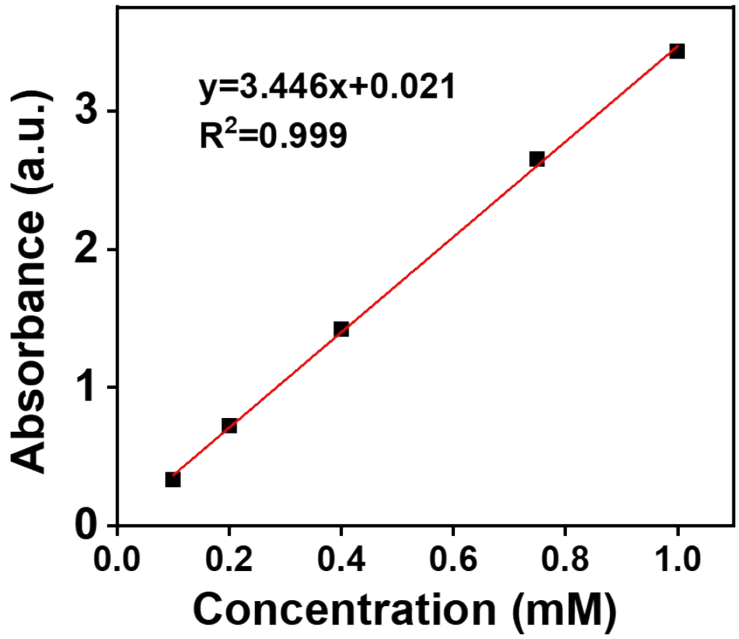

Figure S2 The standard curves of H_2O_2 with varying concentrations ranging from 0.1 to 1 mM.

The Faraday efficiency is calculated according to the following formula:

$$FE(\%) = 2n_{H_2O_2} * \frac{100}{ne^-} = 2Fc_{H_2O_2}V * 100/It$$

Where $^{n_{H_2O_2}}$ is the produced H_2O_2 (mol), ne^- is the electron consumption (mol), F is the Faraday constant (96,485 C mol^{-1}), $^{c_{H_2O_2}}$ is the produced H_2O_2 concentration (mol L^{-1}), V is the volume of catholyte (10.0 mL), I is the current (A), and t is the time (s).

Computational methods: First-principles calculations were carried out on the basis of periodic DFT using a generalized gradient approximation within the Perdew-Burke-Ernzerhof exchange correction functional. We used the projector-augmented wave method for describing ionic cores as implemented in the Vienna ab initio simulation package (VASP). DFT calculations were performed using the Vienna Ab initio Simulation Package (VASP). The wave functions were constructed from the expansion of plane waves with an energy cutoff of 450 eV. Gamma centered k-piont of 3×3×1 have been used for geometry optimization. The consistence tolerances for the geometry optimization are set as 1.0 ×10^{-5} eV/atom for total energy and 0.05 eV/Å for force, respectively. In order to avoid the interaction between the two surfaces, a large vacuum gap of 15 Å has been selected in the periodically repeated slabs.

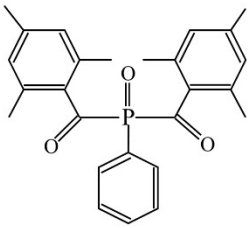

819

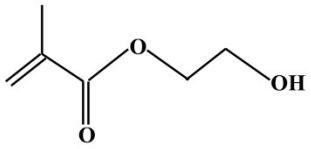

HEMA

Initiators produce free radicals:

$$I \xrightarrow{h\nu} R\cdot$$

Free radicals initiate polymerization of monomers:

$$R\cdot + CH_2{=}CHR \longrightarrow RCH_2C\cdot HR$$

$$RCH_2C\cdot HR + n\,CH_2{=}CHR \longrightarrow R(CH_2CHR)_n\text{-}CH_2\text{-}C\cdot HR$$

$$m\,R(CH_2CHR)_n\text{-}CH_2\text{-}C\cdot HR \longrightarrow \textit{Unreactive species}$$

Figure S3 UV-curing polymerization mechanism.

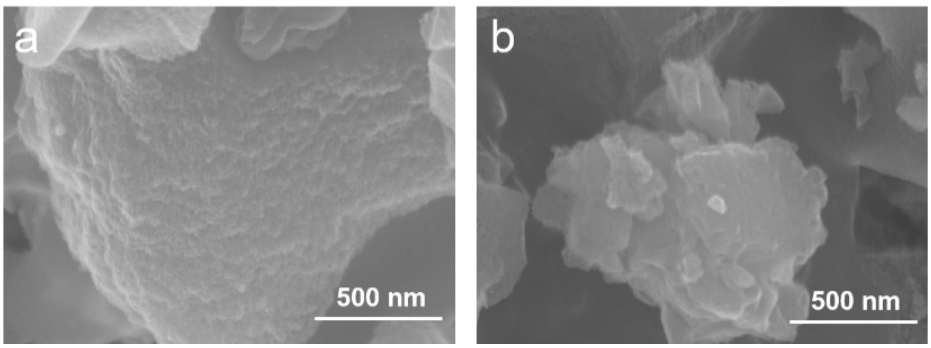

Figure S4 SEM images of (a) porous C and (b) SO_x-porous C.

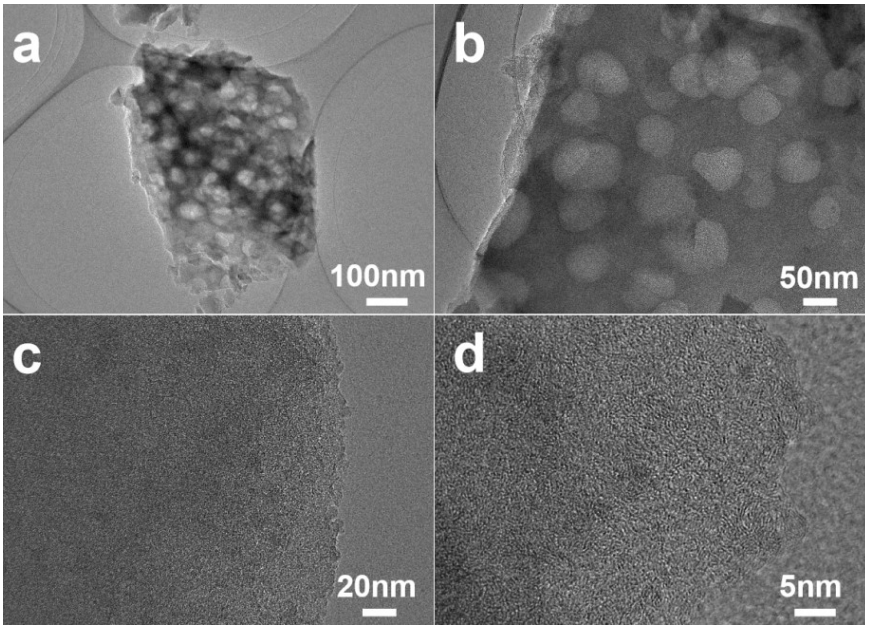

Figure S5 (a-c) TEM image, and (d) HRTEM images of porous C.

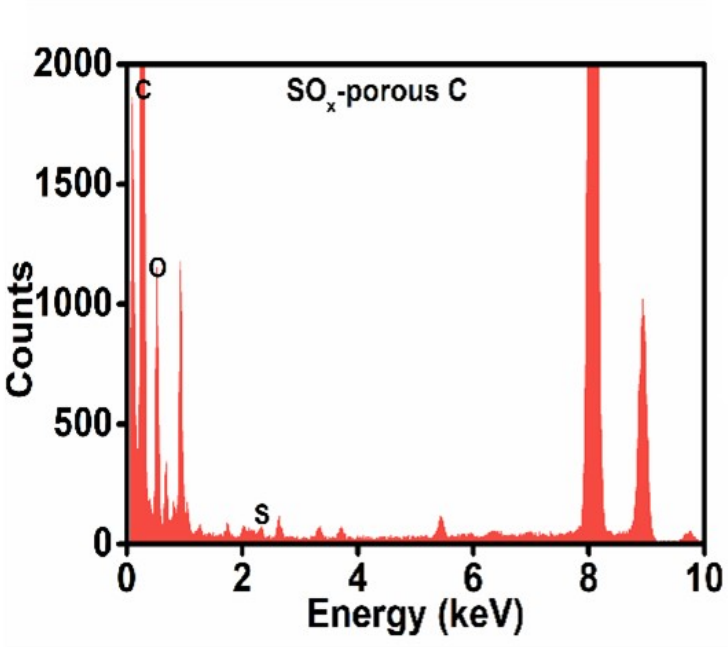

Figure S6 EDX spectrum of SO_x-porous C.

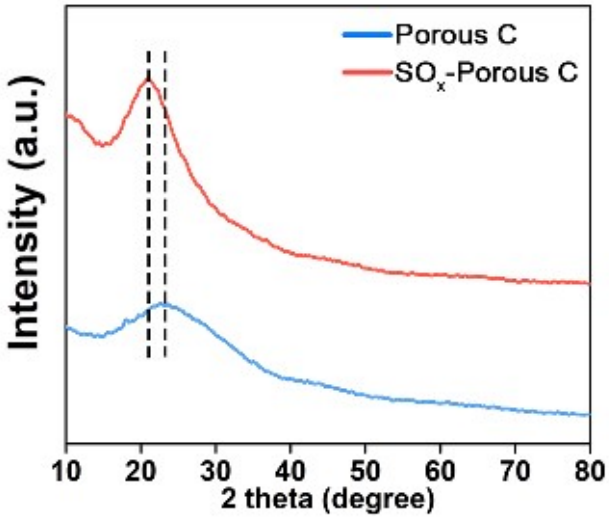

Figure S7 XRD patterns of SO_x-porous C and porous C.

Figure S8 Raman spectra of SO_x-porous C and porous C.

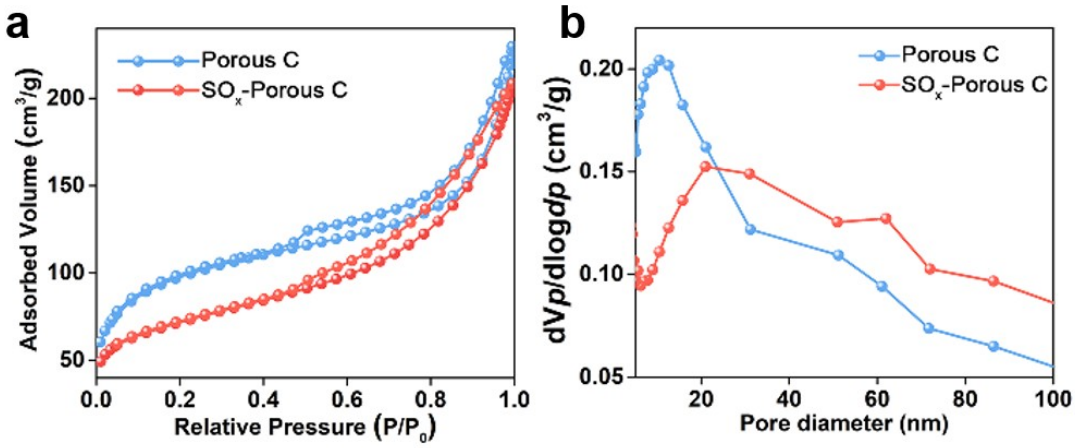

Figure S9 (a) N_2 adsorption/desorption isotherms, (b) the corresponding pore size distribution.

Table S1 Physical properties of porous C and SO_x-porous C.

Sample	Surface area (m^2/g)	Pore volume (cm^3/g)
Porous C	244.55	0.31
SO_x-Porous C	311.96	6.36

Table S2 The mass ratio of C, O, and S element for porous C and SO_x-porous C

	C/%	O/%	S/%
porous C	67.67	32.33	0
SO_x-porous C	70.69	27.68	1.63

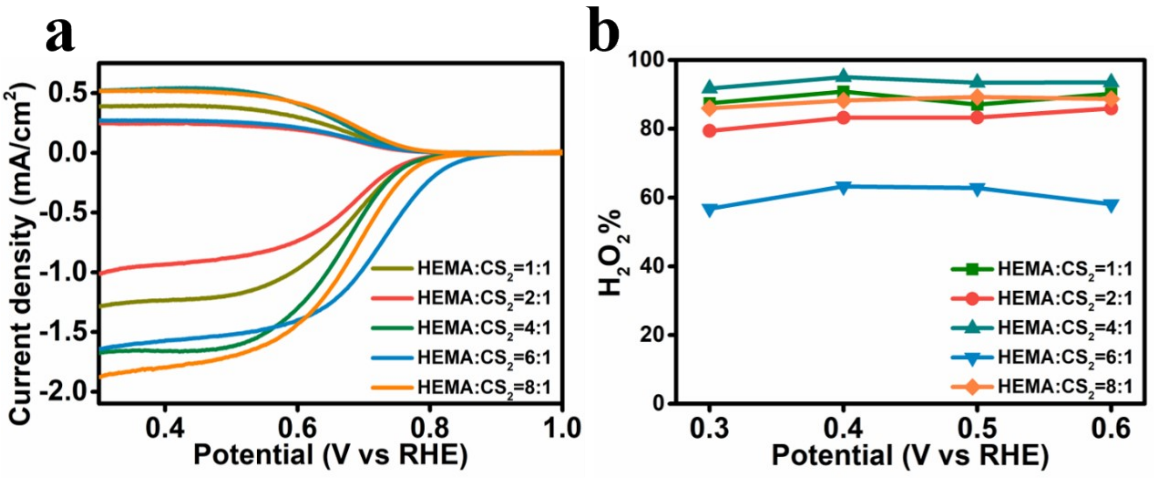

Figure S10 (a) RRDE voltammograms of SO_x-porous C catalysts with different mass ratios of HEMA and CS_2 in O_2-saturated 0.1 M KOH. (b) H_2O_2 selectivity of SO_x-porous C catalysts.

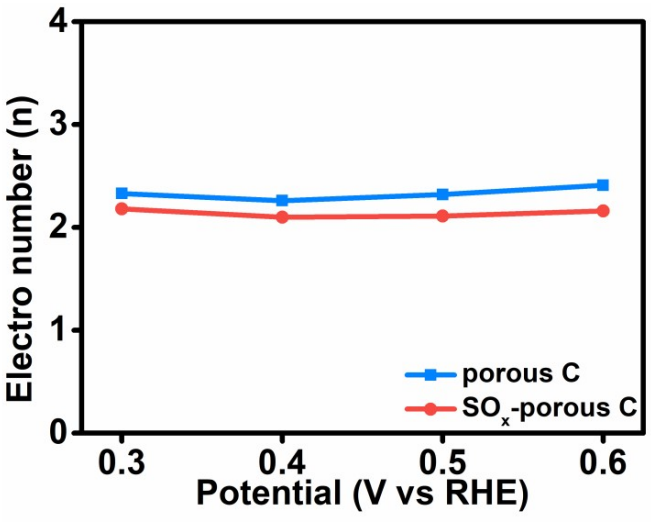

Figure S11 (a) Electron transfer number of of porous C and SO_x-porous C catalysts.

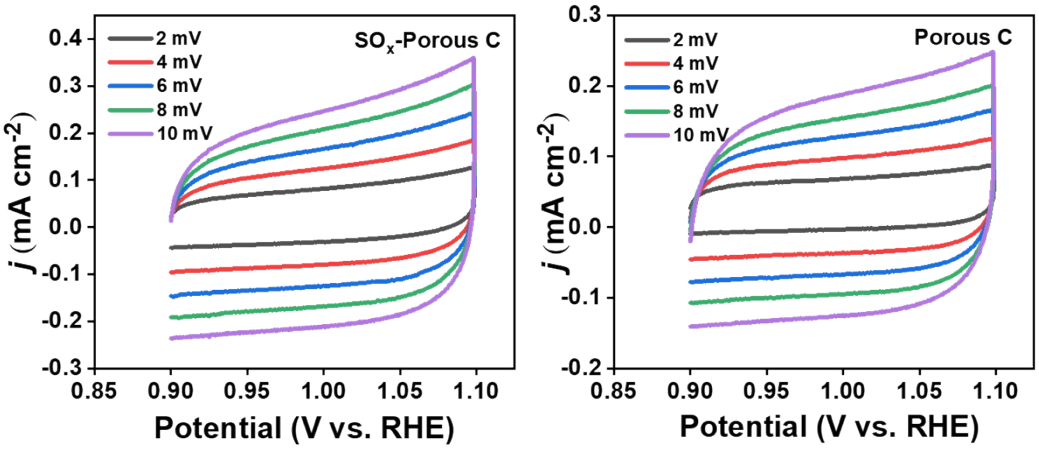

Figure S12 CV curves of SO_x-porous C and porous C at different scan rates.

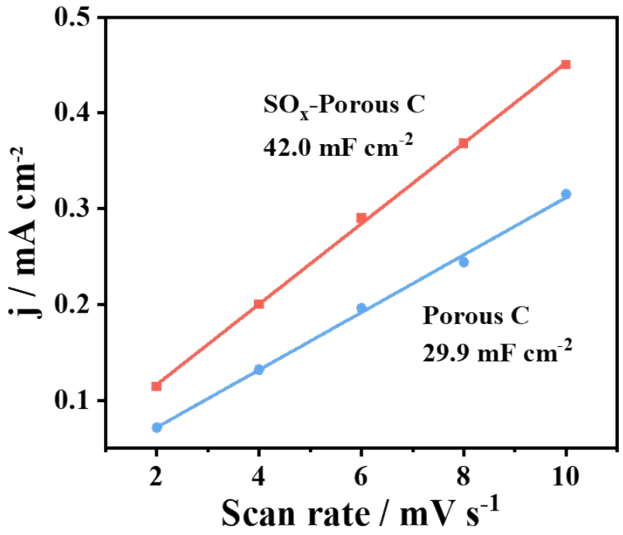

Figure S13 Electrochemically active surface area measurements of SO_x-porous C and porous C.

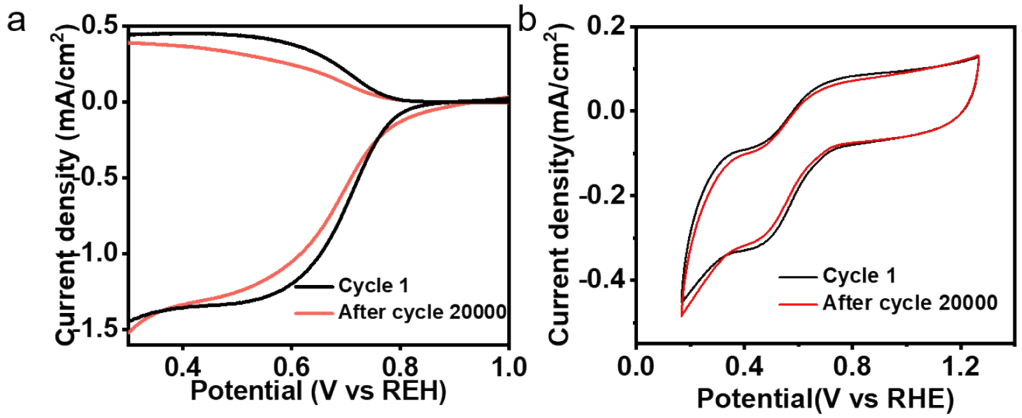

Figure S14 LSV (a) and CV (b) curves of SO_x-porous C after cycles.

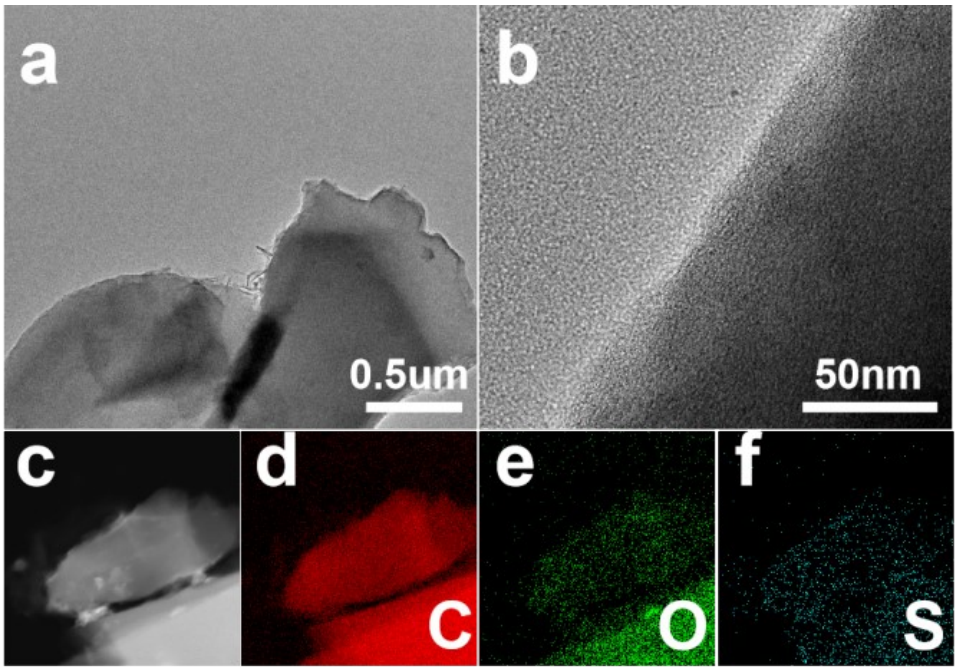

Figure S15 TEM (a), HRTEM (b), STEM (c), and TEM-EDX elemental mapping (d-f) of O, C and S in SO_x-porous C after stability test.

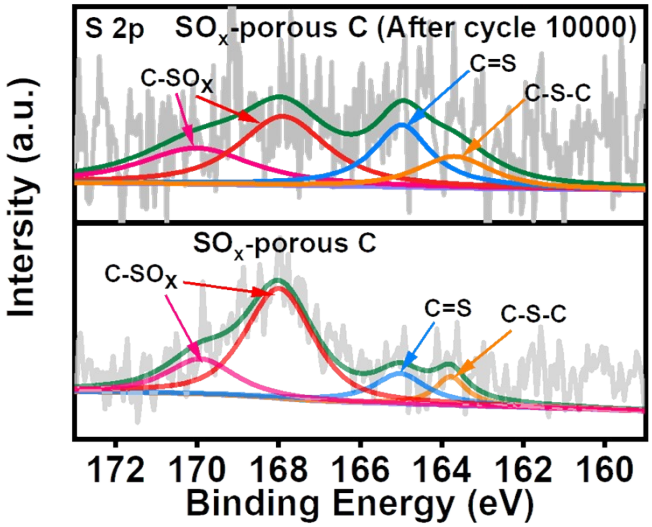

Figure S16 S 2p XPS spectra of SO_x-porous C after 10000 CV cycles of ORR.

Table S3 The mass ratio of S and O element of S-porous C before and after the 10,000 cycles.

Sample	S% (EDS)	O% (EDS)	S% (XPS)	O% (XPS)
Initial	1.83	29.90	1.63	27.68
After cycles	1.50	22.00	1.22	20.10

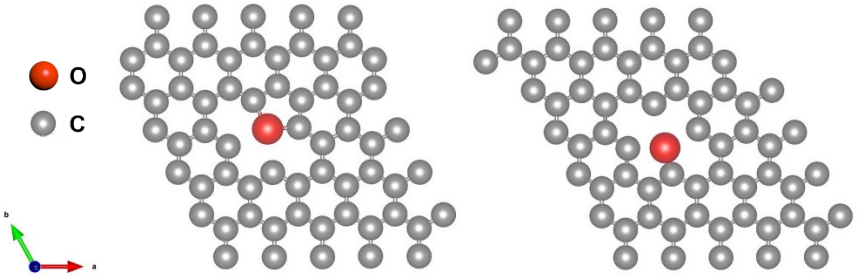

Figure S17 The configurations of C-O and C=O examined in this study.

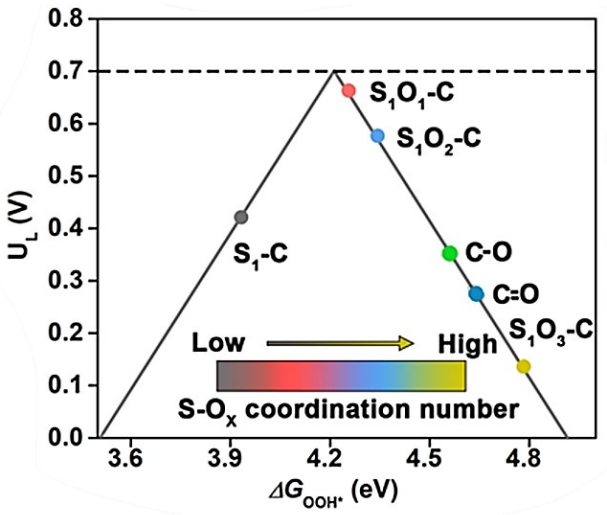

Figure S18 Calculated two-electron ORR-related volcano plot for H_2O_2 formation for the studied configurations.

Table S4 Comparison of 2e⁻ ORR performance for Carbon-based electrocatalysts.

	electrolyte	Potential (V_{RHE})	Selectivity (%)	productivity	Ref.
S-porous C	0.1M KOH	0.3-0.6	~95	604.2 mmol g_{cat}^{-1} h^{-1} (0.5 V vs RHE)	This work
Porous C	0.1M KOH	0.4	~87		This work
O-CNTs	0.1M KOH	0.4-0.65	~90	~3950 mg L^{-1} h^{-1} (50 mA)	[1]
CNTs	0.1M KOH	0.4-0.65	~60		[1]
Commercial Carbon (CMK-3)	0.1M KOH	0.67	90		[2]
Mesoporous defective carbon	0.1M KOH	0.55	80		[3]
Nitrogen-doped carbon	0.1M KOH	0.5	95		[4]
BN-C1	0.1M KOH	0.65	90		[2]
F-mrGO	0.1M KOH	0.75	100	430.8 mmol g_{cat}^{-1} h^{-1} (0.685 V vs RHE)	[2]
GOMC	0.1M KOH	0.72	93	51.3± 4 mg L^{-1} h^{-1} (3 mA)	[5]
HPCS-S	0.1M KOH	0.5	70	183.99 mmol g_{cat}^{-1} h^{-1} (0.3 V vs RHE)	[6]
Fe-CNT	0.1M KOH	0.75	>95		[7]
Co-CNT	0.1M KOH	0.65	74		[7]
Co-POC-O	0.1M KOH	0.6	82	478 mmol g_{cat}^{-1} h^{-1} (100 mA)	[8]
Co_1-NG(O)	0.1M KOH	0.2	~82	418 ± 19 mmol g_{cat}^{-1} h^{-1} (50 mA)	[9]
Mo_1/OSG-H	0.1M KOH	0.3-0.75	95±1		[10]
Co-N/HPC	0.1M KOH	0.5	95	1.7 mol g_{cat}^{-1} h^{-1} (0.5 V vs RHE)	[11]

(PAQS)/CNT	0.1M KOH	0.5	91	86.5 mmol g_{cat}^{-1} h^{-1} (0.5 V vs RHE)	[12]
B-C	0.1M KOH	0.6	90		[13]
NBO-GQDs	0.1M KOH	0.7	90	709 mmol g_{cat}^{-1} h^{-1} (0.7 V vs RHE)	[14]
P-Ni/MC	0.1M KOH	0.15	98	4.4 mol g_{cat}^{-1} h^{-1} (0.15 V vs RHE)	[15]

References

[1] Z. Lu, Chen. G, S. Siahrostami, Z. Chen, K. Liu, J. Xie, L. Liao, T. Wu, D. Lin, Y. Liu, T. F. Jaramillo, J. K. Nørskov, and Y. Cui, Nat Catal., 2018, **1**, 156-162.

[2] H. W. Kim, M. B. Ross, N Kornienko, L. Zhang, J. Guo, P. Yang, and B. D. McCloskey, Nat Catal., 2018, **1**, 282-290.

[3] Y Lee, F Li, K Chang, C. Hu, and T. Ohsaka, Appl Catal B: Environ., 2012, **126**, 208-214.

[4] S Chen, Z Chen, S Siahrostami, D. Higgins, D. Nordlund, D. Sokaras, T. R. Kim, Y. Liu, Xu. Yan, E. Nilsson, R. Sinclair, J. K. Nørskov, T. F. Jaramillo, and Z. Bao, J Am Chem Soc., 2018, **140**, 7851-7859.

[5] Y. J. Sa, J. H. Kim, S. H. Joo. Angew Chem Int Ed., 2019, **58**, 1100-1105.

[6]. G Chen, J Liu, Q Li, P. Guan, X. Yu, L. Xing, J. Zhang, and R. Che, Nano Res, 2019, **12**, 2614-2622.

[7] K Jiang, S Back, A. J. Akey, C. Xia, Y. Hu, W. Liang, D. Schaak, E. Stavitski, J.K. Nørskov, S. Siahrostami, and H. Wang, Nat Commun., 2019, **10**, 3997.

[8] B Li, C Zhao, J Liu, and Q. Zhang, Adv Mater., 2019, **31**, 1808173.

[9] E Jung, H Shin, B. H. Lee, V. Efremov, S. Lee, H. Lee, J. Kim, W. Antink, S. Park, K. Lee, S. Cho, J. Yoo, Y. Sung, and T. Hyeon, Nat Mater., 2020, **19**, 436-442.

[10] C Tang, Y Jiao, B Shi, J. Liu, Z. Xie, X. Chen, Q. Zhang, S. Qiao, Angew Chem Int Ed., 2020, **59**, 9171-9176.

[11] Y Tian, M Li, Z Wu, Q Sun, D Yuan, B Johannessen, L Xu, Y Wang, Y Dou, H Zhao, S Zhang, Angew. Chem. Int. Ed., 2022, **61**, e202213296.

[12] Y Tian, Q Wang, Y Song, J Yang, J Liu, X Liu, and L Zhang, Chem. Commun., 2023, **59**, 4491-4494.

[13] Y Xia, X Zhao, C Xia, Z Wu, P Zhu, J Kim, X Bai, G Gao, Y Hu, J Zhong, Y Liu, and H Wang, Nat Commun., 2021, **12**, 4225.

[14] M Fan, Z Wang, K Sun, A Wang, Y Zhao, Q Yuan, R Wang, J Raj, J Wu, J Jiang, and L Wang, Adv. Mater., 2023, **35**, 2209086.

[15] C Yan, Q Ma, F Wang, L Zhou, X Lv, J Du, B Zheng, and Yong Guo, Chem. Eng. J., 2022, **433**, 133651.